Ergonomics

ISSN: 0014-0139 (Print) 1366-5847 (Online) Journal homepage: http://www.tandfonline.com/loi/terg20

A machine learning approach to detect changes in gait parameters following a fatiguing occupational task

Amir Baghdadi, Fadel M. Megahed, Ehsan T. Esfahani & Lora A. Cavuoto

To cite this article: Amir Baghdadi, Fadel M. Megahed, Ehsan T. Esfahani & Lora A. Cavuoto (2018): A machine learning approach to detect changes in gait parameters following a fatiguing occupational task, Ergonomics, DOI: 10.1080/00140139.2018.1442936

To link to this article: https://doi.org/10.1080/00140139.2018.1442936

Accepted author version posted online: 16 Feb 2018.

Publisher: Taylor & Francis
Journal: *Ergonomics*
DOI: http://doi.org/10.1080/00140139.2018.1442936

A machine learning approach to detect changes in gait parameters following a fatiguing occupational task

Amir Baghdadi [ab], Fadel M. Megahed [c], Ehsan T. Esfahani [b], Lora A. Cavuoto [a]

[a] *Department of Industrial and Systems Engineering, University at Buffalo, The State University of New York, Buffalo, NY 14260, USA;* [b] *Department of Mechanical and Aerospace Engineering, University at Buffalo, The State University of New York, Buffalo, NY 14260, USA;* [c] *Farmer School of Business, Miami University, OH 45056, USA*

Corresponding author's email address: loracavu@buffalo.edu (L. Cavuoto)

Acknowledgements

American Society for Safety Engineers (ASSE) Foundation has supported this study through a grant titled "ASSIST: Advancing Safety Surveillance using Individualized Sensor Technology". The authors would like to acknowledge Justin Vitale, Victoria Queliz, Shaher Yar Jahangir, and Sevack Danadian, undergraduate students at the University at Buffalo who helped us in running the experimental sessions and analyzing the data.

A machine learning approach to detect changes in gait parameters following a fatiguing occupational task

The purpose of this study is to provide a method for classifying *non-fatigued* versus *fatigued* states following manual material handling. A method of template matching pattern recognition for feature extraction (1$ Recognizer) along with the support vector machine (SVM) model for classification were applied on the kinematics of gait cycles segmented by our stepwise search-based segmentation algorithm. A single inertial measurement unit (IMU) on the ankle was used, providing a minimally intrusive and inexpensive tool for monitoring. The classifier distinguished between states using distance-based scores from the recognizer and the step duration. The results of fatigue

detection showed an accuracy of 90% across data from 20 recruited subjects. This method utilizes the minimum amount of data and features from only one low-cost sensor to reliably classify the state of fatigue induced by a realistic manufacturing task using a simple machine learning algorithm that can be extended to real-time fatigue monitoring as a future technology to be employed in the manufacturing facilities.

Practitioner Summary: We examined the use of a wearable sensor for the detection of fatigue-related changes in gait based on a simulated manual material handling task. Classification based on foot acceleration and position trajectories resulted in 90% accuracy. This method provides a practical framework for predicting realistic levels of fatigue.

Keywords: inertial measurement unit (IMU); classification; physical fatigue; wearable sensors

Introduction

Worker fatigue is a highly prevalent phenomenon worldwide. Fatigue prevalence is estimated to be 37.9% in the U.S. workforce (Ricci, Chee, Lorandeau, & Berger, 2007). Worker fatigue is associated with an excess cost of $101 billion in the U.S. (Yung, Bigelow, Hastings, & Wells, 2014). It has been shown that physically demanding work, characterized by forceful exertions, prolonged duration, repetitiveness, and their interactions, places high stresses on the body, which in the absence of rest can result in fatigue (Kumar, 2001). Fatigue and incomplete recovery can reduce capacity, increase injury risk, and decrease work efficiency (Kumar, 2001; Looze, Bosch, & Dieën, 2009; Visser & van Dieën, 2006; Yung et al., 2014). At worst, fatigue can result in accidents and death (Williamson et al., 2011). Significantly reducing the incidence of fatigue-induced workplace injuries depends on accurate and timely detection of fatigue, which can be achieved through the utilization of wearable, minimally invasive sensors for real-time monitoring of fatigue development (Maman, Baghdadi, Megahed, & Cavuoto, 2016).

In this research, we focus on lower extremity muscle fatigue since it is a significant risk factor for slip-induced falls (Lew & Qu, 2014; Parijat & Lockhart, 2008a), which result in approximately 13% of non-fatal workplace injuries in the U.S. (Bureau of Labor Statistics, 2016). Lower extremity fatigue adversely affects proprioception (Gear, 2011; Skinner, Wyatt, Hodgdon, Conard, & Barrack, 1986) and movement coordination (Helbostad, Leirfall, Moe-Nilssen, & Sletvold, 2007) leading to postural instability, motor control impairment, and deviations from normal walking patterns of human gait (Lin et al., 2009; Lockhart et al., 2013; Lu, Megahed, Sesek, & Cavuoto, 2017; Parijat & Lockhart, 2008a; Qu & Yeo, 2011). Furthermore, walking remains a primary activity in manufacturing, construction, agriculture, and other physically demanding occupations, which results in experiencing fatigue in the workers (Zhang, Lockhart, & Soangra, 2014). A survey of manufacturing workers showed an average walking of 5.7 hours in each shift at work and approximately 45% of the workers reported to be fatigued due to the high levels of walking in their jobs (Lu, Megahed, Sesek, & Cavuoto, 2017). Quantitative assessment of the data from inertial measurement unit (IMU) in construction workers shows the ability of kinematics in measuring the level of gait stability as well as the correlation between gait abnormalities and fatigue-induced falls (Jebelli, Ahn, & Stentz, 2015, 2016; Yang, Ahn, Vuran, & Kim, 2017).

To detect lower extremity fatigue, it is important to understand some of its symptoms to

be considered as the modeled features (Baghdadi, Maman, Lu, Cavuoto, & Megahed, 2017). Zhang et al. (2014) reported that lower extremity muscle fatigue resulted in: (a) increased step width, (b) a greater than 2-fold increase in jerk cost, and (c) higher resultant acceleration. Some of the reported differences (especially the step width) by Barbieri, Dos Santos, Lirani-Silva, et al. (2013) were subtle, i.e. may not be easily detectable by a human eye. However, they were identifiable using an IMU placed on the sternum, combined with optical motion capture on the lower extremity. In addition, according to Helbostad et al. (2007), there were significant increases in step width, mediolateral trunk acceleration and step length variability with fatigue. From the results reported by Barbieri, Dos Santos, Lirani-Silva, et al. (2013), Helbostad et al. (2007), and Zhang et al. (2014) the observed changes in gait parameters between *fatigued* and *non-fatigued* states can serve as a basis for continuous monitoring for fatigue detection.

There has been an increasing number of studies that utilize statistical methods and/or data mining methodologies to classify human motion and its associated movement patterns before and after a fatiguing task (Begg & Kamruzzaman, 2005; Helbostad et al., 2007; Kavanagh, Morrison, & Barrett, 2006; Lau, Tong, & Zhu, 2008; Lee, Roan, Smith, & Lockhart, 2009; Parijat & Lockhart, 2008a; Yoshino, Motoshige, Araki, & Matsuoka, 2004; Zhang et al., 2014). Although numerous studies have been devoted to motion analysis, there are limited studies on utilizing kinematic features for the purpose of fatigue detection and how such methods can be applied in different operational environments. There are several reasons for the lack of practical adoption of these methods in detecting fatigue despite its documented importance. First, several of the existing studies are based on motion capture systems and/or force plate measurements (e.g., Begg and Kamruzzaman (2005); Lau et al. (2008); Lee et al. (2009); Strohrmann, Harms, Kappeler-Setz, and Troster (2012)). These systems exclude continuous monitoring outside laboratory environments (Zhang et al., 2014). Second, studies that used IMUs were devoted to distinguishing between extremely *fatigued* and *non-fatigued* states. Their experimental protocols do not mimic typical occupationally-relevant tasks (Helbostad et al., 2007; Yoshino et al., 2004; Zhang et al., 2014). Third, the algorithms used for human movement analysis include complex methods (e.g., the use of Hidden Markov Model (HMM) by Karg, Venture, Hoey, and Kulic (2014)). These algorithms are computationally intensive, require large baseline samples and/or may not be suitable for real-time classification of fatigue.

In this paper, we examine the use of a single IMU, strapped at the right ankle, for continuous monitoring of fatigue symptoms using a template matching pattern recognition technique, along with machine learning algorithms for classifying *non-fatigued* versus *fatigued* states of the human body during walking. The reason for using a single IMU and only on the ankle is to provide a minimally intrusive, inexpensive approach that, if successful, can be used for fatigue detection in the workplace. To achieve this objective, we examine the following research questions:

(1) Can a single IMU placed at the right ankle be sufficient to capture the subtle changes in gait due to fatigue? We examine the ankle since it is, in our opinion, a minimally intrusive location that does not add potential safety risks (e.g. IMUs at the wrist near machinery) and can be used to detect walking steps and/or gait changes.

(2) Can a computationally efficient classifier be used to distinguish between *fatigued* and *non-fatigued* states? We examine the use of the $1 Recognizer to address this question since it is computationally efficient and has been developed for motion (finger gesture)

recognition (Wobbrock, Wilson, & Li, 2007).

Method

We propose a four-step approach, which we summarize in Figure 1 showing the procedure of data collection, data pre-processing, classification, and model evaluation used to meet the objective of classifying *fatigued* vs. *non-fatigued* states. The detailed description of each procedure is provided in the following sections.

[Figure 1 near here]

Data collection

Participants

Fourteen males and six females (mean age 37.1 (17.5) years, mean stature 171.8 (8.6) cm, and mean body mass 76.0 (14.6) kg with the standard deviations presented in the brackets) were recruited to participate in this study from the local workforces and students with some level of manual work. Our focus is on a healthy worker population, so exclusion criteria included reported cardiovascular diseases, musculoskeletal disorders, or a history of injury or pain that would interfere with completion of the experiment. All individuals completed the Physical Activity Readiness Questionnaire (PAR-Q) (Thomas, Reading, & Shephard, 1992) at the start of the session to assess their ability to participate. Study protocols were approved by the University at Buffalo Institutional Review Board and all participants completed an informed consent procedure after being informed about the details of the experiment.

Experimental procedures

Participants completed a three-hour manual material handling (MMH) session, where they continuously palletized and transported several weighted containers. MMH represents a demanding task that occurs frequently in warehousing and shipping operations. The participants were advised to perform the following specific tasks: (a) pick up one of 18 cartons (numbered 1-18, half color-coded blue and half red, and weighing 10, 18, or 26 kg with six cartons in each weight and a random distribution of all factors), (b) place it on a 2-wheeled dolly, (c) walk while pushing the dolly on a set path, and (d) deliver the carton to a prescribed location in a simulated warehouse setup. The detailed sequence of the task, footwear, and floor type (grade resilient tile) are shown in Figure 2. The rectangular-shaped walkway consisted of periods of straight walking, turns on level ground, stops at the beginning and destination, and bending over to load and unload the box onto the dolly. The map of experimental walkway next to the simulated warehouse is provided in Figure 3. This task consisted of three sets of deliveries provided to them on an instruction sheet, based on the carton numbers, color codes, and fragility. The delivery path length for each box was ~80 m and the target timeframe requested to maintain for one delivery set of 18 boxes was 30 minutes. Participants provided a rating of perceived exertion (RPE) on a 6-20 scale (Borg, 1982) every 10 minutes and a rating of subjective fatigue level (SFL) every 30 minutes. The subjective ratings of RPE greater than 10 and SFL greater than 5 at the end of the task were considered to decide on the inclusion of a participant. The experimental

procedure including the samples of raw data for *non-fatigued* and *fatigued* states is illustrated in Figure 4.

[Figure 2 near here]

[Figure 3 near here]

[Figure 4 near here]

The MMH data/experiment are a subset of our larger study presented in Maman, Yazdi, Cavuoto, and Megahed (2017). In our larger study, the participants completed two additional sessions: (a) supply pickup and insertion and (b) parts assembly. Due to the varied nature of the activities, our data collection for the larger study involved the use of three additional IMUs placed at the hip, back of the torso, and wrist, and a heart rate monitor on the chest (Nardolillo, Baghdadi, & Cavuoto, 2017). This paper only focuses on the MMH data since it is the most walking intensive task and thus, presents the opportunity for examining gait kinematics for fatigue detection.

Instrumentation

While performing the task, the participants were instrumented with an IMU placed at the right ankle (Figure 5). The IMU was a Shimmer3 (Shimmer, Dublin, Ireland, www.shimmersensing.com), which is small (51 mm × 34 mm × 14 mm) and equipped with wireless transmission capabilities. The sensor contains a low-noise analog accelerometer, a digital wide range accelerometer, a magnetometer, and a digital gyroscope.

The Shimmer3 device within the body coordinate system (***x y z***) is shown in Figure 5. The dashed lines show the foot trajectory in the Frenet-Serret coordinate system ($\hat{\boldsymbol{e}}_{\boldsymbol{t}}\ \hat{\boldsymbol{e}}_{\boldsymbol{n}}\ \hat{\boldsymbol{e}}_{\boldsymbol{b}}$). This coordinate system describes the kinematics of the foot moving along this 3D trajectory curve. The sagittal frame of each step is expressed by (***A Z N***) axes and (***X Y Z***) is the global frame of reference. The data in the sensor's body frame (***x y z***), were recorded at a sampling rate of 51.2 Hz, which was sufficient for our purpose. Increasing this rate would have resulted in unnecessary large datasets due to the long duration of the experiment. Post-processing and analysis of the signals were performed using Matlab R2015b (MathWorks, USA, www.mathworks.com).

[Figure 5 near here]

Data pre-processing

Kalman filtering

Calibrated data from the sensors were used in a Kalman filter with the assumption of uncorrelated white Gaussian process and measurement noises to estimate the spatial orientation of the body frame with respect to the global frame of reference and ultimately to estimate the kinematics of motion; i.e. jerk (**J**), acceleration (**a**), velocity (**v**), position (**p**), and posture (**θ**). Please note that, these features are a series of magnitudes over time, so are represented as

vectors. Rotation quaternions obtained from the filter over time were used to transform the kinematic data represented in the body coordinate system to the global frame of reference. The Kalman filter was used to calculate the quaternions in two steps. First, the state vector containing the unbiased gyroscope data and filtered attitude were propagated using the dynamics of rotation. In the second step, the state variables were updated using the measured data from the accelerometer.

Using the quaternions, any arbitrary vector $\mathbf{w}_{xyz}$ in the body frame ($x\ y\ z$) can be represented in the global frame of reference ($X\ Y\ Z$) as $\mathbf{w}_{XYZ}$ through the transformation relation. The rotation would be about the unit vector $\hat{\boldsymbol{n}}$ and by angle θ (Diebel, 2006; Pennestri & Valentini, 2010) represented by:

$$\mathbf{w}_{XYZ}(t) = \mathbf{q}(t)\ \mathbf{w}_{xyz}(t)\ \overline{\mathbf{q}}(t), \quad \mathbf{q}(t) = cos\left(\theta(t)/2\right) + sin\left(\theta(t)/2\right)\hat{\boldsymbol{n}}, \tag{1}$$

where $\overline{\mathbf{q}}$ is the quaternion conjugate of $\mathbf{q}$, θ is the rotation angle, and $\hat{\boldsymbol{n}}$ is the unit vector.

The raw measured acceleration data in the body frame ($\mathbf{a}^{m}_{xyz}$) was transformed to the global frame of reference ($\mathbf{a}^{m}_{XYZ}$) and the acceleration data were passed through a 4th order Butterworth low-pass filter with a cutoff frequency of 4 Hz twice, first for each axis to get ($\mathbf{a}^{f}_{XYZ}$) and second after finding the resultant magnitude.

Segmentation

In the next step, the motion segments between a consecutive toe off and heel strike defined by stance points that are known as *strides* need to be identified. To this end, a robust segmentation algorithm was introduced. In this technique, a time window of the magnitude of acceleration data in pure walking containing 50 data points (approximately one second) was selected. This number was selected based on our observations for normal walking speed for each person and may be changed for any other gait speeds accordingly. The proposed stepwise search-based algorithm is shown in (2):

$$\boldsymbol{\Psi}\left(\mathbf{a}^{f}, t_i, t_f\right) = \left\{\underset{t}{\text{argmax}}\ \mathbf{a}^{f}_{XYZ,\,peak}(t_1) \middle|\ t \in [\,t_i,\ t_f]\ \ \mathbf{a}^{f}_{XYZ,\,peak}(t_2)/\mathbf{a}^{f}_{XYZ,\,peak}(t_1) > 1.2\,,\ \ \mathbf{a}^{f}_{XYZ,\,peak}(t) > 5\right\}, \tag{2}$$

where $\boldsymbol{\Psi}(\mathbf{a}^{f})$ are the time points resulted from the stepwise search, t_i and t_f are the starting and ending points of the time window, t_1 includes the first 25 data points and t_2 includes the second 25 data points. In the above equation, $\mathbf{a}^{f}_{XYZ,\,peak}(t)$ is the peak value of the vector $\mathbf{a}^{f}_{XYZ}$ over a specific time period t.

This segmentation algorithm works by considering the existence of two peaks in the translational acceleration of a gait cycle, a larger for heel strike and a smaller for toe off (Tongen & Wunderlich, 2010). After dividing the time window into two equal sub-windows, if the smaller peak resided in the first and larger peak in the second sub-window and the ratio of the peak values was larger than a threshold of 1.2, the larger peak was considered for determination of a valid gait cycle. If not, the search continued until the two peaks met this criterion. The

complementary condition for the acceleration value was a global maximum value higher than 5 m/s^2 for the whole time window. The minimum value of the larger peak and the next 20 points ensuring that the global minimum has been detected is the segmentation point. The acceleration magnitude of 5 m/s^2 is a minimum value for the smaller peak of acceleration magnitude that can certainly be considered for the active phase of a gait pattern knowing that the smaller peak in foot acceleration is reported to be at least 1 **g** (Sabatini, Martelloni, Scapellato, & Cavallo, 2005). Having these time points, we can segment all other motion profiles, e.g., position, velocity, jerk, and posture. The thresholds for segmentation were determined empirically to ensure that the highest accuracy for detecting the gait segments was achieved for all subjects in this level ground walking scenario. Considering that the walking gait data in any other complex scenarios (such as when walking on stairs) always include the two peaks in the waveform of acceleration magnitude, redefining the threshold values accordingly will make the algorithm applicable for these unique cases.

Kinematics Estimation

After removing the gravity vector **g** from the acceleration data represented in the global frame of reference, trapezoidal numerical integration was used to find the velocity. However, there is a significant bias in velocity calculations. Having the acceleration magnitude data segmented into consecutive *strides*, this issue can be addressed, as described below. Jerk was found using a first-order numerical differentiation of acceleration using simple two-point Newton's difference quotient with the step size of $1/51.2$ seconds, and position through the numerical integration of the velocity. The position in the body frame was transferred to the Frenet-Serret coordinate system (i.e., $\mathbf{p}_{\hat{e}_t\,\hat{e}_n\,\hat{e}_b}(t)$) using transformation relation presented in (1) and the quaternions that rotate the direction cosine of body frame to the mean value of direction cosines for the Frenet-Serret coordinate system over a complete gait cycle. Transformation to this coordinate system removes any effect of various sensor orientation on the ankle and provides true foot trajectory in a gait cycle.

The significant bias in the velocity calculated by integrating the accelerations represented in the global frame of reference for each axis is due to the substantial errors in quaternion estimations in Kalman filter (Bergamini et al., 2014) as well as the uncertainties of the gravity vector that deviates from **g** in different geographical locations. In order to minimize these velocity errors, the modified Zero Velocity Update (ZUPT) algorithm introduced by Elwell (1999) and upgraded by Skog, Handel, Nilsson, and Rantakokko (2010) was applied considering that the foot remains stationary for a short period of time between the end of heel strike phase until the start of toe off phase (Ghobadi & Esfahani, 2017). During these stationary periods the magnitude of measured acceleration is equal to **g**. This modified algorithm finds the zero acceleration instances after each acceleration peak point in heel strike by:

$$\left\|\mathbf{a}_{XYZ}^{f}(t_{peak} + t' + \Delta t) - \mathbf{g}\right\| < 5,\ \Delta t = 0\ to\ 0.2 \text{ seconds.} \quad (3)$$

The first value of t' after t_{peak} satisfying the above condition represents the starting time point of the foot stationary state and $t' + 0.2$ seconds is the ending time point. We empirically found that 0.2 seconds is the time period after the bigger peak that assuredly contains the zero

acceleration magnitude. The ZUPT algorithm removes the bias by updating the velocity to be set to zero in the entire stationary period (Ghobadi & Esfahani, 2017).

Fatigue classification

Motion components

An array ($\mathbf{M}_i$) of motion components was introduced containing 8 pairs,

$$\mathbf{M}_i = [(\mathbf{P}_{\hat{e}_t}(\mathrm{t}), \mathbf{P}_{\hat{e}_n}(\mathrm{t})), (\mathbf{t}, \|\mathbf{V}(\mathrm{t})\|), (\mathbf{t}, \|\mathbf{a}(\mathrm{t})\|), (\mathbf{t}, \|\mathbf{J}(\mathrm{t})\|), (\boldsymbol{\theta}_{\boldsymbol{x}}(t), \boldsymbol{\theta}_{\boldsymbol{y}}(t)), (\boldsymbol{\theta}_{\boldsymbol{x}}(t), \dot{\boldsymbol{\theta}}_{\boldsymbol{x}}(t)), (\boldsymbol{\theta}_{\boldsymbol{y}}(t), \dot{\boldsymbol{\theta}}_{\boldsymbol{y}}(t)),(\boldsymbol{\theta}_{\boldsymbol{z}}(t), \dot{\boldsymbol{\theta}}_{\boldsymbol{z}}(t))\ ], \quad (4)$$

where ($\mathbf{P}_{\hat{e}_t}(\mathrm{t}), \mathbf{P}_{\hat{e}_n}(\mathrm{t})$) is the 2D position trajectory in Frenet-Serret coordinate system, ($\mathbf{t}, \|\mathbf{V}(\mathrm{t})\|$) is the profile of velocity magnitude versus time, ($\mathbf{t}, \|\mathbf{a}(\mathrm{t})\|$) is the profile of acceleration magnitude versus time, ($\mathbf{t}, \|\mathbf{J}(\mathrm{t})\|$) is the profile of jerk magnitude versus time, and ($\boldsymbol{\theta}_{\boldsymbol{x}}(t), \boldsymbol{\theta}_{\boldsymbol{y}}(t)$), ($\boldsymbol{\theta}_{\boldsymbol{x}}(t), \dot{\boldsymbol{\theta}}_{\boldsymbol{x}}(t)$), ($\boldsymbol{\theta}_{\boldsymbol{y}}(t), \dot{\boldsymbol{\theta}}_{\boldsymbol{y}}(t)$) and ($\boldsymbol{\theta}_{\boldsymbol{z}}(t), \dot{\boldsymbol{\theta}}_{\boldsymbol{z}}(t)$) are the profiles of angular position and angular velocity in ($\boldsymbol{x}\ \boldsymbol{y}\ \boldsymbol{z}$) coordinate system. Each component segment was normalized starting from zero, and a motion template is defined by a single segment of any of the pairs in the motion component array, e.g., $\mathbf{T}_k = \left(\mathbf{M}_i^k(1), \mathbf{M}_i^k(2)\right) = \left(\mathbf{P}_{\hat{\boldsymbol{e}}_t}^k(\mathrm{t}), \mathbf{P}_{\hat{\boldsymbol{e}}_n}^k(\mathrm{t})\right)$, where *k* represents the component segments as one gait step.

Motion templates of each motion component are expected to have a different pattern in the *fatigued* and *non-fatigued* states. This might not necessarily be visibly distinguishable; however, they can be recognized properly by means of finding the score-based point-to-point distance between templates.

Training data

A set of 2000 sample data points (~40 seconds) containing pure walking were manually extracted from the first 10 minutes of the experiment after warmup, to make sure the participants are completely accustomed to the task. This data set was identified as *non-fatigued*. A similar procedure was applied for the last 10 minutes of data and identified as *fatigued* by considering an SFL of greater than 5 as a criterion. After segmentation of these two sets, batches of 25 *strides* were selected from each set as *fatigued* and *non-fatigued* training sets to get the Euclidean distance-based scores as one feature for the final classification by comparing each testing *stride* with both training batches in $1 Recognizer (Wobbrock et al., 2007).

Euclidean distance-based scores

Similar to the training part, two unique sets of ~40 seconds and two batches of 25 *strides* within the sets were extracted from the first and the last 10 minutes as the testing sets without any overlap with the training sets. Having an equal number of *strides* in both *fatigued* and *non-fatigued* states avoids the biased classification towards any of the states. Next, the testing batches of *strides* were concatenated together making an even pool of data. Then, one *stride* in each

template was randomly selected from the pool and passed through the modified $1 Recognizer classifier along with each of the two *fatigued* and *non-fatigued* training batches of *strides*. This is a computationally simple algorithm with universal applications for gesture and pattern recognition which provides higher accuracies than other classifiers such as Dynamic Time Warping (DTW) (Myers & Rabiner, 1981; Tappert, Suen, & Wakahara, 1990) and Rubine (Rubine, 1991). In addition, there is no need for the numerous training samples required for other sophisticated classifiers that have been used for this application (e.g., HMM (Anderson, Bailey, & Skubic, 2004; Cao & Balakrishnan, 2005; Sezgin & Davis, 2005), neural networks (Pittman, 1991), and statistical classifiers (Cho, 2006)). In $1 Recognizer, a score was assigned by comparing the testing *stride* and each *stride* in the training batches based on the pointwise Euclidean distance between the selected testing segment and each of the *fatigued* and *non-fatigued* training segment classes. Please refer to Wobbrock et al. (2007) for more details on $1 Recognizer algorithm.

Support vector machine (SVM) classification

For each test *stride*, the mean of distance-based scores calculated in $1 Recognizer and the test *stride* duration were considered as *feature data points* for distinguishing between the two classes. A binary SVM classifier using Radial Basis kernel function (RBF) was then applied to the score and step duration *feature data points* of 50 random test *strides*. The kernel parameter was optimized on the training data set and the values that maximize the classification rate were selected. In this step of classification, 20% of the *feature data points* were held out as testing and the SVM was trained based on the rest of the *feature data points* and for testing the classifier, the testing data points were utilized. In order to validate the classifier, a 5-fold cross-validation was applied on each subject data in which the 50 *feature data points* were randomly partitioned into five subgroups of equal sizes. In addition to the results for each motion template, a simple ensemble classification result was also provided through majority voting of predictions by templates such that more than four votes for the number of "*fatigued"* labeled templates were considered as *fatigued.* It is assumed that the fusing of the classification results will provide more accurate results as well as a better holistic picture of the state of the subject since the eight templates are inherently different from a kinematics perspective.

Model Evaluation

Model evaluation is the final step in the *fatigue classification model* in which the accuracy of the classifier was assessed. Three evaluating measures were considered for assessing the error rate (accuracy), the probability of correct *fatigued* state detection (sensitivity), and the probability of correct *non-fatigued* state detection (specificity) for all motion templates as well as their combination.

Results

The mean (SD) value for the subjective ratings of RPE and SFL across the whole participants were 14.4 (2.6) and 6.8 (1.2), respectively, that were used to identify the existence of a *fatigued* state in a participant.

The sample segmentation results of highly filtered acceleration magnitude to be prepared for segmentation for *non-fatigued* and *fatigued* states are shown in Figure 6, after setting the recognized stationary periods to zero. This profile belongs to the training sets of a 29-year old female participant with SFL of 7.

[Figure 6 near here]

The mean trajectory of four different motion templates from the training sets is presented in Figure 7. The distinction between the *fatigued* and *non-fatigued* states is shown in the separate profiles with the shaded region representing the standard deviation. There is a distinct decrease in the step length after inducing fatigue. In addition, the mean profiles of velocity magnitude, acceleration magnitude, and jerk magnitude show a decrease in step duration. The other comparable quantity is the peak value of these four mean trajectories. The graphical representation shows a decrease in the maximum step height and velocity magnitude after fatigue. The graphs also show that differences between the profile of mean trajectories for other kinematical variables (i.e., acceleration magnitude $\|\mathbf{a}\|$, and jerk magnitude $\|\mathbf{J}\|$) among *fatigued* and *non-fatigued* states are not as visually clear as the position and velocity magnitude trajectories.

[Figure 7 near here]

We provide the SVM classification results of all eight motion components and the combination of them using a simple vote ensemble in Table 1. It is noteworthy that the classification was tested multiple times to show the repeatability of the algorithm. The combination of all templates was found to have the highest accuracy (90%) for correctly detection of the *fatigued* state as it was assumed. The acceleration template has the second highest accuracy (89%), which can be attributed to the accurate direct segmentation results and the fact that it was the directly collected, rather than calculated, measure since the kinematic computations can be a source of error and uncertainty. The next highest performing templates were position trajectory and velocity magnitude both with an accuracy of (86%). In addition, the templates containing angular properties show a meaningful change in the leg posture in the sagittal plane ($\boldsymbol{\theta}_x$, $\dot{\boldsymbol{\theta}}_x$). It is noteworthy that for assessing the performance of the classifier in a case of fewer training data, instead of having two equal data sets for testing and training, we also investigated 40% and 60% of training data and the results were not compromised.

[Table 1 near here]

Discussion

Our findings indicate that fatigue induced by a simulated manufacturing task results in changes in temporal and spatial characteristics of gait kinematics including step length and step duration that can be used for fatigue detection. Our distance-based template matching algorithm was able to predict the *fatigued* and *non-fatigued* states with the highest accuracy of 90% for the

combination of all templates across 20 subjects.

Fatigue-induced changes in human gait kinematics have been reported in several studies (Barbieri, dos Santos, Vitório, van Dieën, & Gobbi, 2013; Dingwell, Joubert, Diefenthaeler, & Trinity, 2008; Janssen et al., 2011; Karg et al., 2014; Parijat & Lockhart, 2008a, 2008b; Qu & Yeo, 2011; Yaggie & McGregor, 2002; Zhang et al., 2014). However, there are discrepancies in the results of human gait kinematics variability by these different studies that can be associated mainly with different fatiguing protocols. The most common protocols of fatigue generation that have been studied include running on a treadmill (Qu & Yeo, 2011), sit-to-stand tasks (Barbieri, dos Santos, Vitório, et al., 2013; Yaggie & McGregor, 2002), or applying maximum voluntary contraction (MVC) until exhaustion such that the subject cannot continue the task (Barbieri, Lee, Gobbi, Pijnappels, & Van Dieën, 2013). Different protocols may affect different muscles, e.g., medial-lateral muscles in running and anterior-posterior muscles in sit-to-stand tasks, causing different motor responses (Qu & Yeo, 2011).

Here we report the results of human gait characteristics from these studies and highlight our classification results in the case of each kinematic metric. Regarding the walking trajectory characteristics, based on the results for a number of studies (e.g., Barbieri, Dos Santos, Lirani-Silva, et al. (2013); Barbieri, dos Santos, Vitório, et al. (2013); Barbieri, Lee, et al. (2013) and Morris, Cantwell, Vowels, and Dodd (2002)), step length decreases due to fatigue. They interpreted this decrease as a result of applying a proactive mechanism to modulate the effector system for adapting to environmental conditions (Gérin-Lajoie, Richards, & McFadyen, 2005). In terms of walking velocity, the difference between *fatigued* and *non-fatigued* groups was not significant as reported by Zhang et al. (2014). On the other hand, subjects significantly increased their step velocity following fatigue according to Barbieri, dos Santos, Vitório, et al. (2013) and Barbieri, Lee, et al. (2013). Walking velocity can affect the friction by altering the coefficient of friction through changing the ratio of horizontal to vertical foot force and controlling the likelihood of slip-induced falls (Karst, Hageman, Jones, & Bunner, 1999; Lockhart, Woldstad, & Smith, 2003; Mills & Barrett, 2001; Parijat & Lockhart, 2008a). Even with the inconsistencies in gait kinematics variations resulting from fatigue reported in the previous studies, our classification algorithm was able to properly discern these changes and detect the fatigue states using these two features with 86% accuracy. In addition, Parijat and Lockhart (2008a) and Yoshino et al. (2004) reported a significant change in acceleration magnitude. Furthermore, Lockhart et al. (2013) results show an increase in heel contact jerk in post-fatigue walking. Our fatigue detection method could classify the changes in acceleration and jerk magnitude with 89% and 85% accuracies, respectively.

These kinematic changes of motion component trajectories are not the same for all templates. The distinction in the position template of ($\mathbf{P}_{\hat{e}_t}$, $\mathbf{P}_{\hat{e}_n}$) provided in Figure 7 is clear from the mean trajectory graphs, however, for acceleration magnitude component, the segments are more precise and truly represent one gait cycle due to the direct segmentation of the acceleration rather than using the segment points, which allows for better distinction between classes. The SVM classifier is applied on two features, one being step duration which always changed following fatigue. Considering this feature along with any other feature (e.g., jerk) ameliorates the low performance of the second feature and boosts the classification results for all motion templates. Rotational features, including the combinations of leg angular positions and velocities (i.e., ($\boldsymbol{\theta}_x$, $\boldsymbol{\theta}_y$), ($\boldsymbol{\theta}_x$, $\dot{\boldsymbol{\theta}}_x$)), provide good results in classification, indicating that leg posture and the pattern of walking in the sagittal plane changes following fatigue, which has not been addressed in any of the previous studies.

Human movement analysis and human activity recognition have been studied by various algorithms including SVM, HMM, neural network, discriminant analysis, or nearest neighbor (Karg et al., 2014). Classification between normal and post-exhaustion gait patterns have been studied by Janssen et al. (2011) and Karg et al. (2008) with the report of a significant difference in gait kinematics of pre- and post-exhaustion. However, as is typical in human fatigue detection studies, large inter-subject variance in gait characteristics highly affects the classification accuracy (Janssen et al., 2011).

A summary of the classification methods from the previous studies, along with their results of fatigue detection during gait is provided in Table 2. Zhang et al. (2014) examined different SVM classifiers where the results for linear and RBF kernel function show a better performance. Their best results in terms of accuracy, sensitivity, and specificity outperform ours, which can be attributed mainly to their larger number of features employed, the procedure of fatigue inducement, and the number of sensors utilized. On the other hand, we had better performance in fatigue detection than Karg et al. (2014) in spite of their more complex classification method and selection of features. One-to-one comparison of the fatigue detection studies may not seem appropriate since the protocols and data used vary among studies. However, as a general comparison, this study has some advantages. First, in contrast to other similar works that utilized costly motion capture systems or data from multiple sensors in the whole duration of fatigue inducement protocol, this study used the data of short periods (~40 seconds) in *fatigued* and *non-fatigued* states from only one IMU attached to the ankle. This feature enables the method to be used in real-time applications by extracting a single *stride*, calculating the motion components, and plugging these into the trained classifier to predict the state of fatigue. The time required for accomplishing this purpose is approximately 3.6 seconds using a personal computer, which is a sufficient time for fatigue prediction purposes. Second, workplace simulated fatigue inducement tasks were used for data collection in this study, however, most of the other studies considered extreme exercises until complete exhaustion as their protocols. In other words, changes in the parameters studied in a realistic fatigue inducement task may not be as significant as they might have been had the changes happened through extreme exercise.

[Table 2 near here]

There are some limitations associated with this study. The subjects recruited for the experiments consisted of both manufacturing and non-industrial workers, which can affect their induced fatigue level depending on how accustomed they are to the fatiguing task. Moreover, the time of experimental sessions was not randomized in each day, which would have removed the effect of time on fatigue development. In addition, the level of fatigue was not as extreme as an eight-hour shift in a real manufacturing environment, which may have limited the level of induced fatigue. The task was also equivalent for all subjects, regardless of strength or gender, which may differ from a real manufacturing condition. Lastly, although this study lacked physiological validation (e.g., electromyography (EMG) measurement to support the presence of muscle fatigue), which limited our ability to confirm the detection of fatigue, subjective ratings of RPE and SFL were used as a measure for this confirmation. Nevertheless, physiological validation, as a standard, will be considered in future experimental studies. Despite these limitations to generalizability, this study provides a robust classification method to be applied to future tests in a real manufacturing environment and in conditions that address these issues.

Supplementary Materials

The data and MATLAB codes for this study are accessible through the following GitHub Repository: https://github.com/AmirBGitHub/fatigue-gait-classification

Conclusion

The reported method uses a template matching pattern recognition technique, along with machine learning algorithms for classifying *non-fatigued* versus *fatigued* states of the human body during walking using an IMU attached to the ankle. A robust and easy to implement segmentation method for gait cycle detection is proposed for a highly accurate detection of consecutive gait cycles. The classification was carried out using an RBF SVM on the distance-based score of segmented gait cycles and step duration as the two features. The results indicate that the combination of all motion components yields the highest accuracy of 90% in predicting the fatigue states for the 20 recruited subjects. We found that the fatigue due to a simulated manufacturing task of manual material handling results in changes in gait kinematics. Not all of the gait kinematics perform the same in fatigue prediction such that the foot acceleration and position trajectories are among the high performing parameters. This method provides a practical framework for predicting realistically-induced fatigue through manufacturing tasks, which can be extended to real-time fatigue monitoring due to the simplicity of this template matching technique.

References

Anderson, D., Bailey, C., & Skubic, M. (2004). Hidden Markov Model symbol recognition for sketch-based interfaces. *AAAI fall symposium*, 15-21.

Baghdadi, A., Maman, Z. S., Lu, L., Cavuoto, L. A., & Megahed, F. M. (2017). Effects of Task Type, Task Duration, and Age on Body Kinematics and Subjective Fatigue. *Proceedings of the Human Factors and Ergonomics Society Annual Meeting, 61*(1), 1040-1040.

Barbieri, F. A., Dos Santos, P. C. R., Lirani-Silva, E., Vitório, R., Gobbi, L. T. B., & Van Diëen, J. H. (2013). Systematic review of the effects of fatigue on spatiotemporal gait parameters. *Journal of back and musculoskeletal rehabilitation, 26*(2), 125-131.

Barbieri, F. A., dos Santos, P. C. R., Vitório, R., van Dieën, J. H., & Gobbi, L. T. B. (2013). Effect of muscle fatigue and physical activity level in motor control of the gait of young adults. *Gait & posture, 38*(4), 702-707.

Barbieri, F. A., Lee, Y.-J., Gobbi, L. T. B., Pijnappels, M., & Van Dieën, J. H. (2013). The effect of muscle fatigue on the last stride before stepping down a curb. *Gait & posture, 37*(4), 542-546.

Begg, R., & Kamruzzaman, J. (2005). A machine learning approach for automated recognition of movement patterns using basic, kinetic and kinematic gait data. *Journal of biomechanics, 38*(3), 401-408.

Bergamini, E., Ligorio, G., Summa, A., Vannozzi, G., Cappozzo, A., & Sabatini, A. M. (2014). Estimating orientation using magnetic and inertial sensors and different sensor fusion approaches: accuracy assessment in manual and locomotion tasks. *Sensors, 14*(10), 18625-18649.

Borg, G. A. (1982). Psychophysical bases of perceived exertion. *Med sci sports exerc, 14*(5), 377-381.

Bureau of Labor Statistics. (2016). *Nonfatal occupational injuries and illnesses requiring days away from work*. Retrieved from http://www.bls.gov/news.release/pdf/osh2.pdf.

Cao, X., & Balakrishnan, R. (2005). Evaluation of an on-line adaptive gesture interface with command prediction. *Proceedings of Graphics Interface 2005*, 187-194.

Cho, M. G. (2006). A new gesture recognition algorithm and segmentation method of Korean scripts for gesture-allowed ink editor. *Information Sciences, 176*(9), 1290-1303.

Diebel, J. (2006). Representing attitude: Euler angles, unit quaternions, and rotation vectors. *Matrix, 58*(15-16), 1-35.

Dingwell, J. B., Joubert, J. E., Diefenthaeler, F., & Trinity, J. D. (2008). Changes in muscle activity and kinematics of highly trained cyclists during fatigue. *IEEE Transactions on Biomedical Engineering, 55*(11), 2666-2674.

Elwell, J. (1999). *Inertial navigation for the urban warrior.* Paper presented at the AeroSense'99.

Gear, W. S. (2011). Effect of different levels of localized muscle fatigue on knee position sense. *Journal of Sports Science and Medicine, 10*(4), 725-730.

Gérin-Lajoie, M., Richards, C. L., & McFadyen, B. J. (2005). The negotiation of stationary and moving obstructions during walking: anticipatory locomotor adaptations and preservation of personal space. *Motor control, 9*(3), 242-269.

Ghobadi, M., & Esfahani, E. T. (2017). A Robust Automatic Gait Monitoring Approach Using a Single IMU for Home-Based Applications. *Journal of Mechanics in Medicine and Biology, 17*(05), 1750077.

Helbostad, J. L., Leirfall, S., Moe-Nilssen, R., & Sletvold, O. (2007). Physical fatigue affects gait characteristics in older persons. *The Journals of Gerontology Series A: Biological Sciences and Medical Sciences, 62*(9), 1010-1015.

Janssen, D., Schöllhorn, W. I., Newell, K. M., Jäger, J. M., Rost, F., & Vehof, K. (2011). Diagnosing fatigue in gait patterns by support vector machines and self-organizing maps. *Human movement science, 30*(5), 966-975.

Jebelli, H., Ahn, C. R., & Stentz, T. L. (2015). Comprehensive fall-risk assessment of construction workers using inertial measurement units: Validation of the gait-stability metric to assess the fall risk of iron workers. *Journal of Computing in Civil Engineering, 30*(3), 04015034.

Jebelli, H., Ahn, C. R., & Stentz, T. L. (2016). Fall risk analysis of construction workers using inertial measurement units: Validating the usefulness of the postural stability metrics in construction. *Safety Science, 84*, 161-170.

Karg, M., Kühnlenz, K., Buss, M., Seiberl, W., Tusker, F., Schmeelk, M., & Schwirtz, A. (2008). Expression and automatic recognition of exhaustion in natural walking. *IADIS Int. Conf. Interfaces and Human Computer Interaction (IHCI)*, 165-172

Karg, M., Venture, G., Hoey, J., & Kulic, D. (2014). Human movement analysis as a measure for fatigue: A hidden Markov-based approach. *IEEE Transactions on Neural Systems and Rehabilitation Engineering, 22*(3), 470-481.

Karst, G. M., Hageman, P. A., Jones, T. F., & Bunner, S. H. (1999). Reliability of foot trajectory measures within and between testing sessions. *The Journals of Gerontology Series A: Biological Sciences and Medical Sciences, 54*(7), M343-M347.

Kavanagh, J. J., Morrison, S., & Barrett, R. S. (2006). Lumbar and cervical erector spinae fatigue elicit compensatory postural responses to assist in maintaining head stability during walking. *Journal of Applied Physiology, 101*(4), 1118-1126.

Kumar, S. (2001). Theories of musculoskeletal injury causation. *Ergonomics, 44*(1), 17-47.

Lau, H.-Y., Tong, K.-Y., & Zhu, H. (2008). Support vector machine for classification of walking conditions using miniature kinematic sensors. *Medical & biological engineering & computing, 46*(6), 563-573.

Lee, M., Roan, M., Smith, B., & Lockhart, T. E. (2009). Gait analysis to classify external load conditions using linear discriminant analysis. *Human movement science, 28*(2), 226-235.

Lew, F. L., & Qu, X. (2014). Effects of multi-joint muscular fatigue on biomechanics of slips. *Journal of biomechanics, 47*(1), 59-64.

Lin, D., Nussbaum, M. A., Seol, H., Singh, N. B., Madigan, M. L., & Wojcik, L. A. (2009). Acute effects of localized muscle fatigue on postural control and patterns of recovery during upright stance: influence of fatigue location and age. *European journal of applied physiology, 106*(3), 425-434.

Lockhart, T. E., Soangra, R., Chung, C., Frames, C., Fino, P., & Zhang, J. (2013). Development of automated gait assessment algorithm using three inertial sensors and its reliability. *Biomedical sciences instrumentation, 50*, 297-306.

Lockhart, T. E., Woldstad, J. C., & Smith, J. L. (2003). Effects of age-related gait changes on the biomechanics of slips and falls. *Ergonomics, 46*(12), 1136-1160.

Looze, M. d., Bosch, T., & Dieën, J. v. (2009). Manifestations of shoulder fatigue in prolonged activities involving low-force contractions. *Ergonomics, 52*(4), 428-437.

Lu, L., Megahed, F. M., Sesek, R. F., & Cavuoto, L. A. (2017). A survey of the prevalence of fatigue, its precursors and individual coping mechanisms among US manufacturing workers. *Applied ergonomics, 65*, 139-151.

Maman, Z. S., Baghdadi, A., Megahed, F., & Cavuoto, L. (2016). Monitoring and Change Point Estimation of Normal (In-Control) and Fatigued (Out-of-Control) State in Workers. *ASME 2016 International Design Engineering Technical Conferences and Computers and Information in Engineering Conference, 3*,

V003T011A011-V003T011A011. doi:10.1115/DETC2016-60487
Maman, Z. S., Yazdi, M. A. A., Cavuoto, L. A., & Megahed, F. M. (2017). A data-driven approach to modeling physical fatigue in the workplace using wearable sensors. *Applied ergonomics, 65*(53), 515-529.
Mills, P. M., & Barrett, R. S. (2001). Swing phase mechanics of healthy young and elderly men. *Human movement science, 20*(4), 427-446.
Morris, M. E., Cantwell, C., Vowels, L., & Dodd, K. (2002). Changes in gait and fatigue from morning to afternoon in people with multiple sclerosis. *Journal of Neurology, Neurosurgery & Psychiatry, 72*(3), 361-365.
Myers, C. S., & Rabiner, L. R. (1981). A comparative study of several dynamic time-warping algorithms for connected-word recognition. *Bell System Technical Journal, 60*(7), 1389-1409.
Nardolillo, A. M., Baghdadi, A., & Cavuoto, L. A. (2017). Heart Rate Variability During a Simulated Assembly Task; Influence of Age and Gender. *Proceedings of the Human Factors and Ergonomics Society Annual Meeting, 61*(1), 1853-1857.
Parijat, P., & Lockhart, T. E. (2008a). Effects of lower extremity muscle fatigue on the outcomes of slip-induced falls. *Ergonomics, 51*(12), 1873-1884.
Parijat, P., & Lockhart, T. E. (2008b). Effects of quadriceps fatigue on the biomechanics of gait and slip propensity. *Gait & posture, 28*(4), 568-573.
Pennestrì, E., & Valentini, P. (2010). Dual quaternions as a tool for rigid body motion analysis: A tutorial with an application to biomechanics. *Archive of Mechanical Engineering, 57*(2), 187-205.
Pittman, J. A. (1991). Recognizing handwritten text. *Proceedings of the SIGCHI conference on Human factors in computing systems Reaching through technology, CHI '91*, 271-275. doi:10.1145/108844.108914
Qu, X., & Yeo, J. C. (2011). Effects of load carriage and fatigue on gait characteristics. *Journal of biomechanics, 44*(7), 1259-1263.
Ricci, J. A., Chee, E., Lorandeau, A. L., & Berger, J. (2007). Fatigue in the US workforce: prevalence and implications for lost productive work time. *Journal of Occupational and Environmental Medicine, 49*(1), 1-10.
Rubine, D. (1991). Specifying gestures by example. *Proceedings of the 18th annual conference on Computer graphics and interactive techniques, 25*(4), 329-337 doi:10.1145/122718.122753
Sabatini, A. M., Martelloni, C., Scapellato, S., & Cavallo, F. (2005). Assessment of walking features from foot inertial sensing. *IEEE Transactions on biomedical engineering, 52*(3), 486-494.
Sezgin, T. M., & Davis, R. (2005). HMM-based efficient sketch recognition. *Proceedings of the 10th international conference on Intelligent user interfaces*, 281-283. doi:10.1145/1040830.1040899
Skinner, H., Wyatt, M., Hodgdon, J., Conard, D., & Barrack, R. (1986). Effect of fatigue on joint position sense of the knee. *Journal of Orthopaedic Research, 4*(1), 112-118.
Skog, I., Handel, P., Nilsson, J.-O., & Rantakokko, J. (2010). Zero-velocity detection—An algorithm evaluation. *IEEE Transactions on Biomedical Engineering, 57*(11), 2657-2666.
Strohrmann, C., Harms, H., Kappeler-Setz, C., & Troster, G. (2012). Monitoring kinematic changes with fatigue in running using body-worn sensors. *IEEE transactions on information technology in biomedicine, 16*(5), 983-990.
Tappert, C. C., Suen, C. Y., & Wakahara, T. (1990). The state of the art in online handwriting recognition. *IEEE Transactions on pattern analysis and machine intelligence, 12*(8), 787-808.
Thomas, S., Reading, J., & Shephard, R. J. (1992). Revision of the Physical Activity Readiness Questionnaire (PAR-Q). *Canadian journal of sport sciences, 17*(4), 338-345.
Tongen, A., & Wunderlich, R. E. (2010). Biomechanics of running and walking. *Mathematics and Sports, 43*.
Visser, B., & van Dieën, J. H. (2006). Pathophysiology of upper extremity muscle disorders. *Journal of Electromyography and Kinesiology, 16*(1), 1-16.
Williamson, A., Lombardi, D. A., Folkard, S., Stutts, J., Courtney, T. K., & Connor, J. L. (2011). The link between fatigue and safety. *Accident Analysis & Prevention, 43*(2), 498-515.
Wobbrock, J. O., Wilson, A. D., & Li, Y. (2007). Gestures without libraries, toolkits or training: a $1 recognizer for user interface prototypes. *Proceedings of the 20th annual ACM symposium on User interface software and technology*, 159-168. doi:10.1145/1294211.1294238
Yaggie, J. A., & McGregor, S. J. (2002). Effects of isokinetic ankle fatigue on the maintenance of balance and postural limits. *Archives of physical Medicine and Rehabilitation, 83*(2), 224-228.
Yang, K., Ahn, C. R., Vuran, M. C., & Kim, H. (2017). Collective sensing of workers' gait patterns to identify fall hazards in construction. *Automation in Construction, 82*, 166-178.
Yoshino, K., Motoshige, T., Araki, T., & Matsuoka, K. (2004). Effect of prolonged free-walking fatigue on gait and physiological rhythm. *Journal of biomechanics, 37*(8), 1271-1280.

Yung, M., Bigelow, P. L., Hastings, D. M., & Wells, R. P. (2014). Detecting within-and between-day manifestations of neuromuscular fatigue at work: an exploratory study. *Ergonomics, 57*(10), 1562-1573.
Zhang, J., Lockhart, T. E., & Soangra, R. (2014). Classifying lower extremity muscle fatigue during walking using machine learning and inertial sensors. *Annals of biomedical engineering, 42*(3), 600-612.

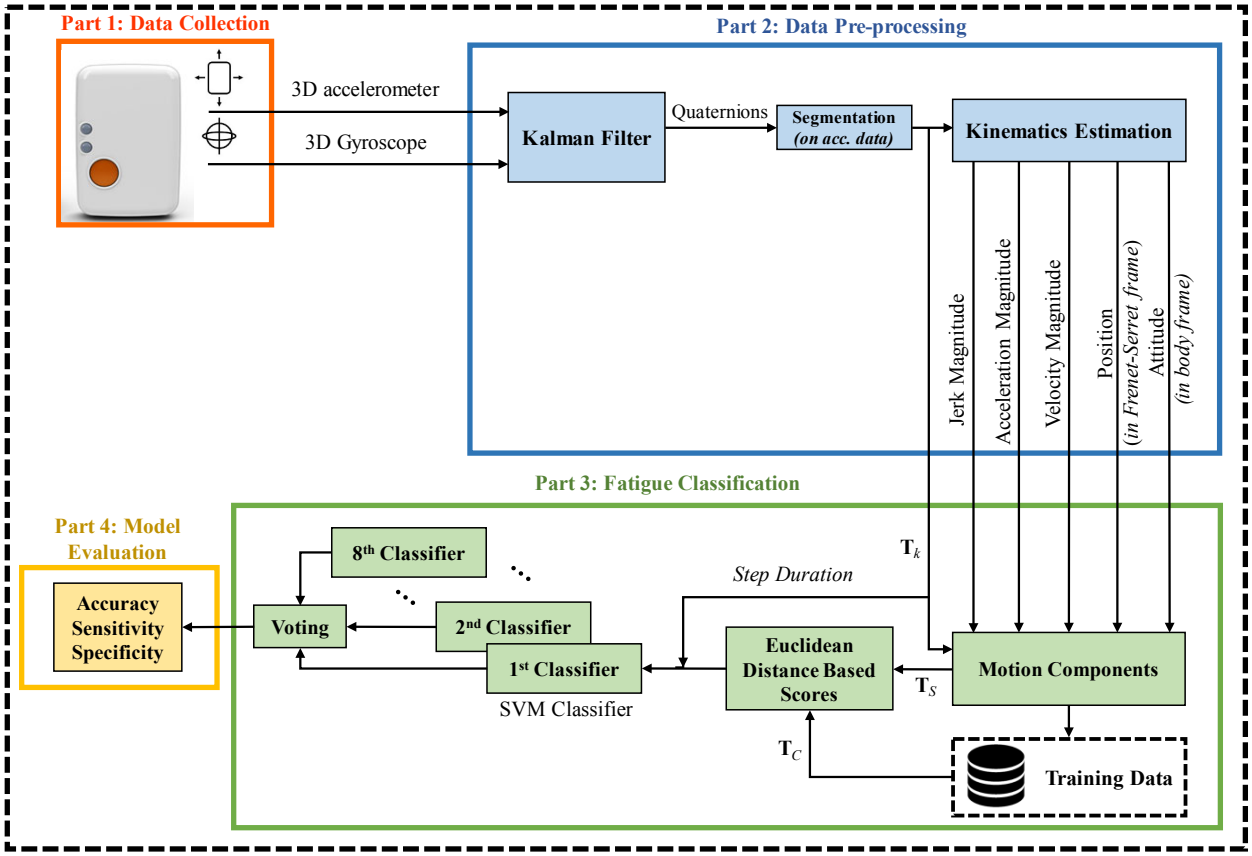

Figure 1. The block diagram of the proposed fatigue classification model. The procedure includes data collection, data pre-processing, classification, and model evaluation.

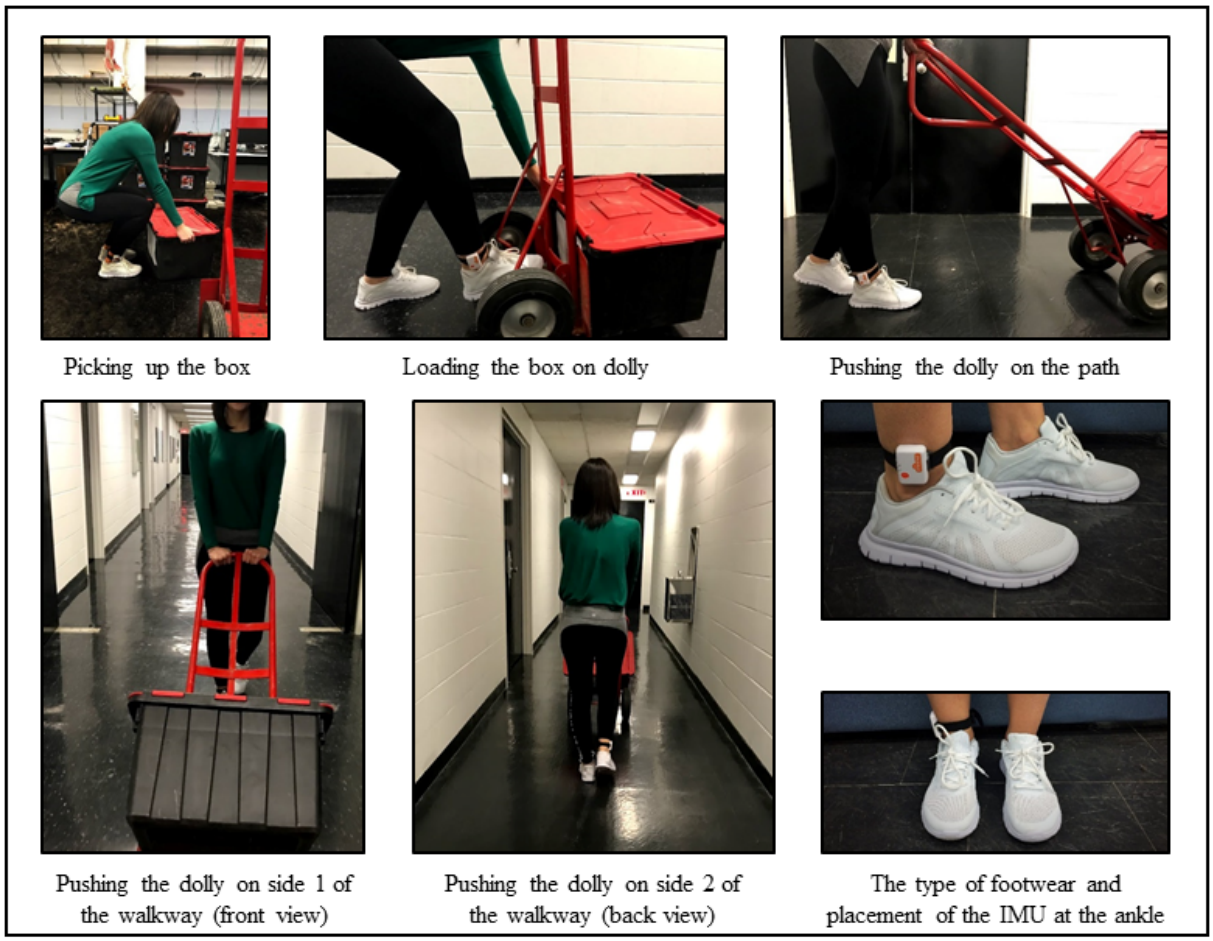

Figure 2. The detailed sequence of task along with the floor type demonstration as grade resilient tile. The bottom right corner images show the type of footwear and the placement of IMU at the ankle.

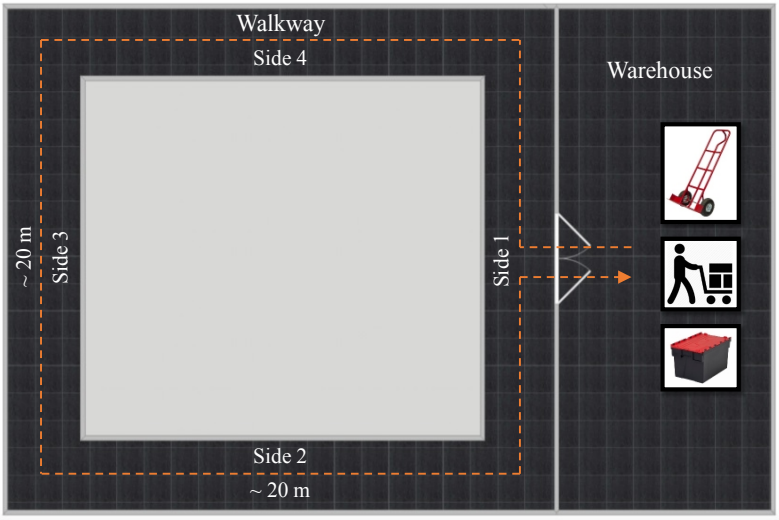

Figure 3. The map of experiment walkway next to the warehouse for stacking the boxes using a dolly. The walkway had a rectangular shape that included straight walks and turns on level ground. The delivery path length for each box was ~80 m.

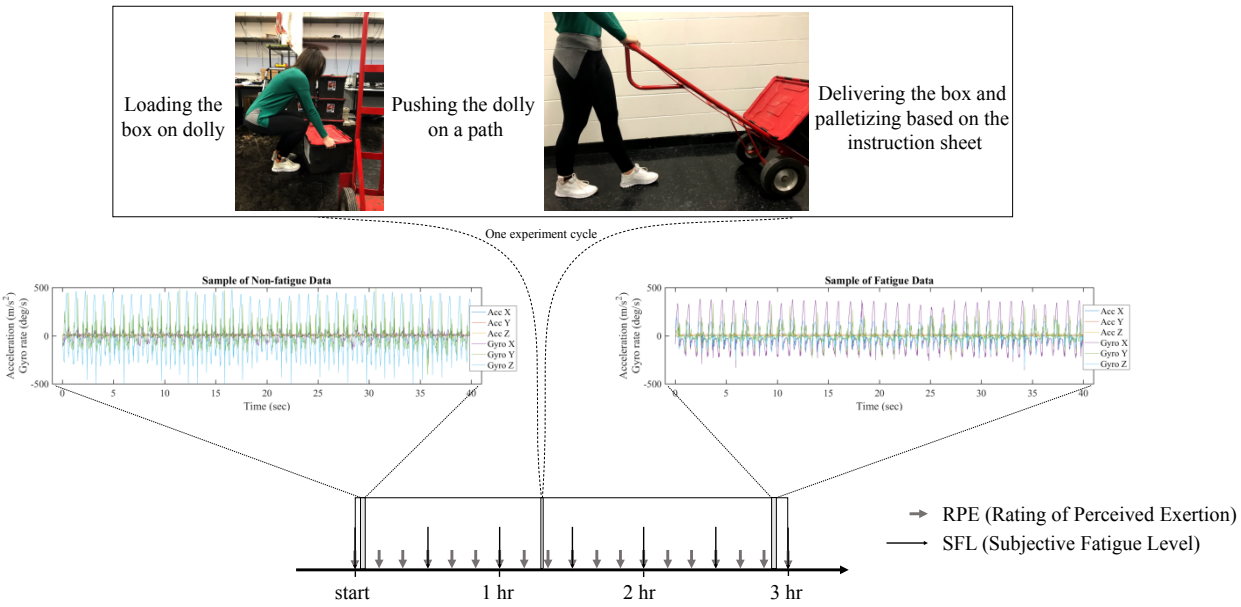

Figure 4. The timeline of the experimental procedure with sample data and illustration of one experiment cycle

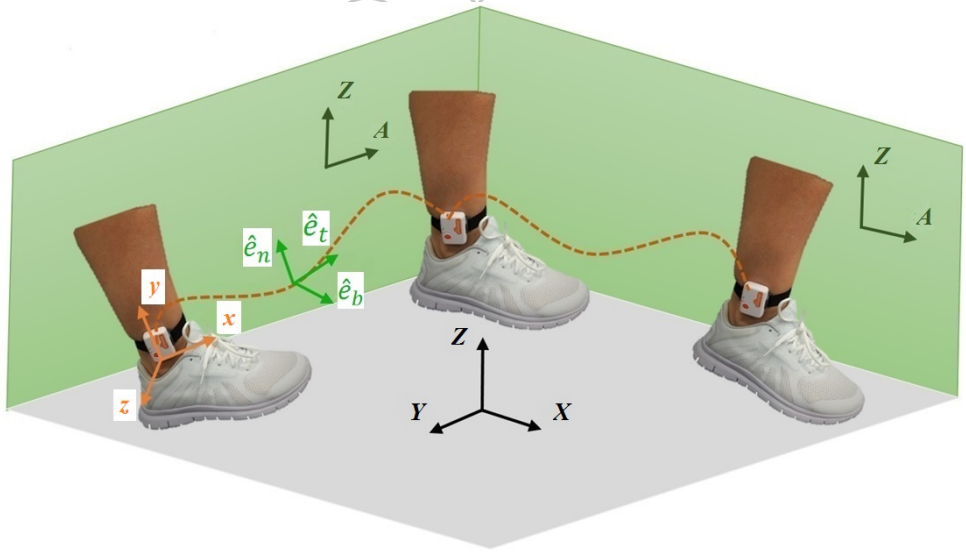

Figure 5. Illustration of the coordinate systems used including IMU body coordinate system (***x y z***), Frenet-Serret coordinate system ($\hat{\boldsymbol{e}}_{\boldsymbol{t}}\ \hat{\boldsymbol{e}}_{\boldsymbol{n}}\ \hat{\boldsymbol{e}}_{\boldsymbol{b}}$), global frame of reference (***X Y Z***), and the sagittal frame of each step (***A Z N***).

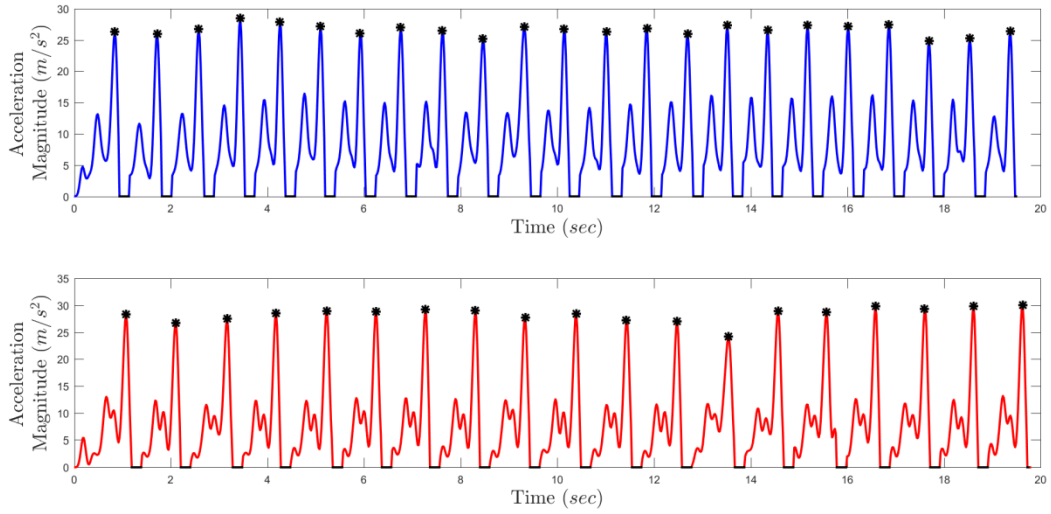

Figure 6. The segmented acceleration magnitude for *non-fatigued* (blue line) and *fatigued* (red line) states, peak points representing heel strike (black *), and rest periods (black line).

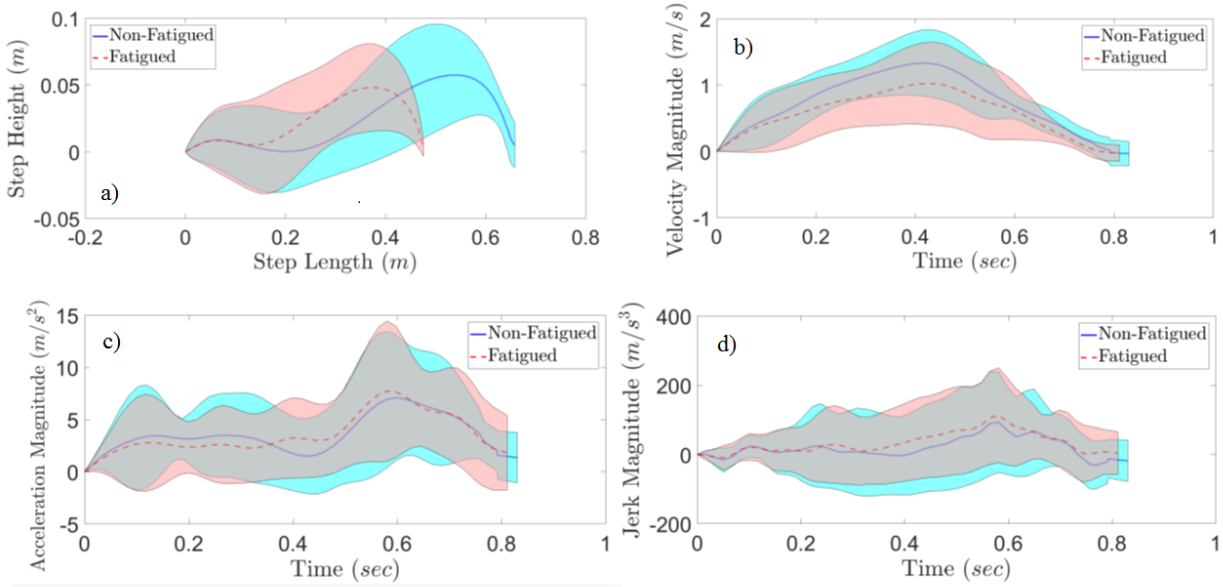

Figure 7. Mean trajectory and standard deviation as the shaded areas for different motion components (a) positions in $\hat{\boldsymbol{e}}_{\boldsymbol{t}}$ and $\hat{\boldsymbol{e}}_{\boldsymbol{n}}$ ($\mathbf{P}_{\hat{\boldsymbol{e}}_{\boldsymbol{t}}}(t)$, $\mathbf{P}_{\hat{\boldsymbol{e}}_{\boldsymbol{n}}}(t)$) (b) velocity magnitude ($\mathbf{t}$, $\|\mathbf{V}(t)\|$) (c) acceleration magnitude ($\mathbf{t}$, $\|\mathbf{a}(t)\|$) (d) jerk magnitude ($\mathbf{t}$, $\|\mathbf{J}(t)\|$)

Table 1. Accuracy, sensitivity, and specificity of classifier using Euclidean distances based on different templates

	$(\mathbf{P}_{\hat{e}_t}(t), \mathbf{P}_{\hat{e}_n}(t))$	$(\mathbf{t}, \|\mathbf{V}(t)\|)$	$(\mathbf{t}, \|\mathbf{a}(t)\|)$	$(\mathbf{t}, \|\mathbf{J}(t)\|)$	$(\boldsymbol{\theta}_x(t), \boldsymbol{\theta}_y(t))$	$(\boldsymbol{\theta}_x(t), \dot{\boldsymbol{\theta}}_x(t))$	$(\boldsymbol{\theta}_y(t), \dot{\boldsymbol{\theta}}_y(t))$	$(\boldsymbol{\theta}_z(t), \dot{\boldsymbol{\theta}}_z(t))$	**Combination of all templates**
Accuracy	0.86	0.86	0.89	0.85	0.84	0.84	0.82	0.80	**0.90**
Sensitivity	0.89	0.86	0.90	0.87	0.85	0.82	0.85	0.80	**0.87**
Specificity	0.84	0.87	0.89	0.83	0.85	0.86	0.81	0.81	**0.92**

Table 2. Summary of classification methods and results of fatigue detection in gait

	Fatigue Inducement Protocol	Classification Method	Features Used	Reported Results
Zhang et al. (2014)	Squatting Exercise until Exhaustion	RBF SVM	Resultant, Mean, Maximum, Minimum, Range, Skewness, Energy and Dominant Frequency for Acceleration and Jerk in Trunk using IMU	Highest Accuracy: 0.96 Highest Sensitivity: 0.98 Highest Specificity: 0.98
Janssen et al. (2011)	Isokinetic Leg Exercises with Weights until Exhaustion	RBF SVM Self-organizing Maps (SOM)	Deviation from average for the profile of Ground Reaction Force	Highest Accuracy: 0.98
Karg et al. (2014)	Squatting Exercise until Exhaustion	Parametric Hidden Markov Model (PHMM) / Linear Regression	Time Series of Angles and Angular Velocities / Minimum, Mean, Maximum, and ROM for Joint Angles and Temporal Features using Motion Capture System	Highest Accuracy: 0.81
Karg et al. (2008)	Maximum Power Test on a Rowing Ergometer until Exhaustion	Linear Discriminant Analysis (LDA), Naive Bayes, K-Nearest Neighbor Clustering (KNN) and SVM	Structural and Dynamical cues by Principal Component Analysis (PCA) and Fourier Transformation (FT) on Marker Position Data and Joint Angles using Motion Capture System	Highest Accuracy: 1.00
Maman et al. (2017)	Manufacturing Fatiguing Tasks including Parts Assembly, Supply Pickup and Insertion, and Manual Material Handling	Penalized Logistic Regression and Penalized Regression	Descriptive Statistics as well as Percent Change and Cumulative Sum (CUSUM) for each Statistic using Heartrate Sensor and 4 IMUs	Highest Sensitivity: 1.00 Highest Specificity: 0.79